Supporting Information for

Droplet Evaporation Dynamics of Low Surface Tension Fluids Using the Steady Method

A. Alperen Günay[1,*], Marisa Gnadt[1], Soumyadip Sett[1], Hamed Vahabi[2], Arun K. Kota[3], Nenad Miljkovic[1,4,5,6,*]

[1]*Department of Mechanical Science and Engineering, University of Illinois at Urbana – Champaign, 1206 W Green St, Urbana, Illinois 61801 USA*

[2]*Department of Biomedical Engineering, Duke University, Durham, NC 27708, USA*

[3]*Department of Mechanical and Aerospace Engineering, North Carolina State University, Raleigh, NC 27695, USA*

[4]*Department of Electrical and Computer Engineering, University of Illinois at Urbana – Champaign, 1206 W Green St, Urbana, Illinois 61801 USA*

[5]*Materials Research Laboratory, University of Illinois, Urbana, Illinois 61801, USA*

[6]*International Institute for Carbon Neutral Energy Research (WPI-I2CNER), Kyushu University, 744 Motooka, Nishi-ku, Fukuoka 819-0395, Japan*

* Corresponding Author. E-mail address: nmiljkov@illinois.edu, gunay@photon.t.u-tokyo.ac.jp

S.1. Surface Fabrication, Functionalization and Characterization

S.1.1. Surface Fabrication. A 20 nm thick Al_2O_3 diffusion barrier and a 5 nm thick film of Fe catalyst layer were deposited on silicon growth substrates using electron beam deposition to grow CNT by chemical vapor deposition (CVD). The silicon substrate was heated to 750°C in a 2.54 cm quartz furnace and annealed for 3 min under a flow of H_2 and He at 400 and 100 sccm, respectively; after being purged in He/H_2 atmosphere in a 2.54 cm quartz furnace for 15 min. Randomly aligned CNTs were then grown by flowing C_2H_4 at 200 sccm for 1 min. The characteristic diameter of the thermally grown CNT was $d \approx 7$ nm[1].

Commercially available (Cu) tabs (99.9% purity, 25 mm x 25 mm x 0.8 mm) were used to create CuO nanostructures. Each Cu tab was thoroughly rinsed with acetone, ethanol, isopropyl alcohol (IPA), and deionized (DI) water; followed by dipping 2.0 M Hydrochloric acid solution for 2 min to remove native oxide film on the surface, rinsing with DI water and drying with nitrogen gas Nanostructured CuO films were formed by immersing the cleaned tabs in hot (96 $\pm$ 3 ˚C) alkaline solution composed of $NaClO_2$, NaOH, $Na_3PO_4{\cdot}12H_2O$, and DI water (3.75:5:10:100 wt%). This process resulted in the formation of an initial thin (≈300 nm) Cu_2O layer which reoxidizes to form sharp, knife-like CuO oxide structures ($L_h \approx 1\mu m$).

S.1.2. Surface Functionalization. To obtain a hydrophobic silicon substrate**,** the initial silicon substrate was thoroughly cleaned by rinsing it with acetone, methanol, ethanol, isopropyl alcohol (IPA) and deionized (DI) water to prepare it for liquid phase deposition (LPD). After drying the substrate with nitrogen gas, it was plasma cleaned for 10 minutes. A drop of trichloroperfluorooctyl-silane (TFTS, CAS no. 78560-45-9, Sigma Aldrich) was added to 500 mL hexane, and the resulting solution was vigorously mixed before placing the clean silicon substrate inside the solution. The coated silicon substrate (referred to as Si-HTMS in the text)

was removed from the solution after 24 hours and was rinsed with ethanol and DI water and dried in nitrogen gas. For hydrophilic functionalization, the plasma cleaned silicon substrates were sputter coated with gold having 10 nm thickness (referred to as Si-Au in the text).

To obtain a superhydrophobic substrate, nanostructured CuO tab was initially dried in clean nitrogen gas to prepare it for LPD. Then, a solution containing a single drop of heptadecafluorodecyltrimethoxysilane (HTMS, CAS no. 83048-65-1, Sigma Aldrich) in 500 mL of hexane was prepared and vigorously mixed, before placing the CuO tab in it. The coated Cu tab (referred to as Cu-HTMS in the text) was removed from the solution after 24 hours, rinsed with ethanol, DI water and dried with clean nitrogen gas before placing it in an atmospheric oven at 80 °C for 90 mins.

S.1.3. Surface Characterization. A microgoniometer (MCA-3, Kyowa Interface Science) was used to perform contact angle measurements of ≈100 nL droplets on all samples.

S.2. Dispensed Monodisperse Microdroplets

In order to find the rate of evaporation when the evaporating droplet becomes steady, we need to possess information on the frequency of deposition and the average size of the dispensed droplet. Thus, we performed imaging analysis for the working fluids of interest (water, ethanol, hexane and dodecane) under certain conditions to obtain the volumetric information we need. Our analyses yielded the radii information for the dispensed monodisperse droplets for each working fluid ($R = 8.77 \pm 0.56$ μm for water [Figure S1a], $R = 16.47 \pm 1.73$ μm for ethanol [Figure S1b], $R = 12.67 \pm 0.22$ μm for hexane [Figure S1c] and $R = 5.37 \pm 0.57$ μm for dodecane [Figure S1d]).

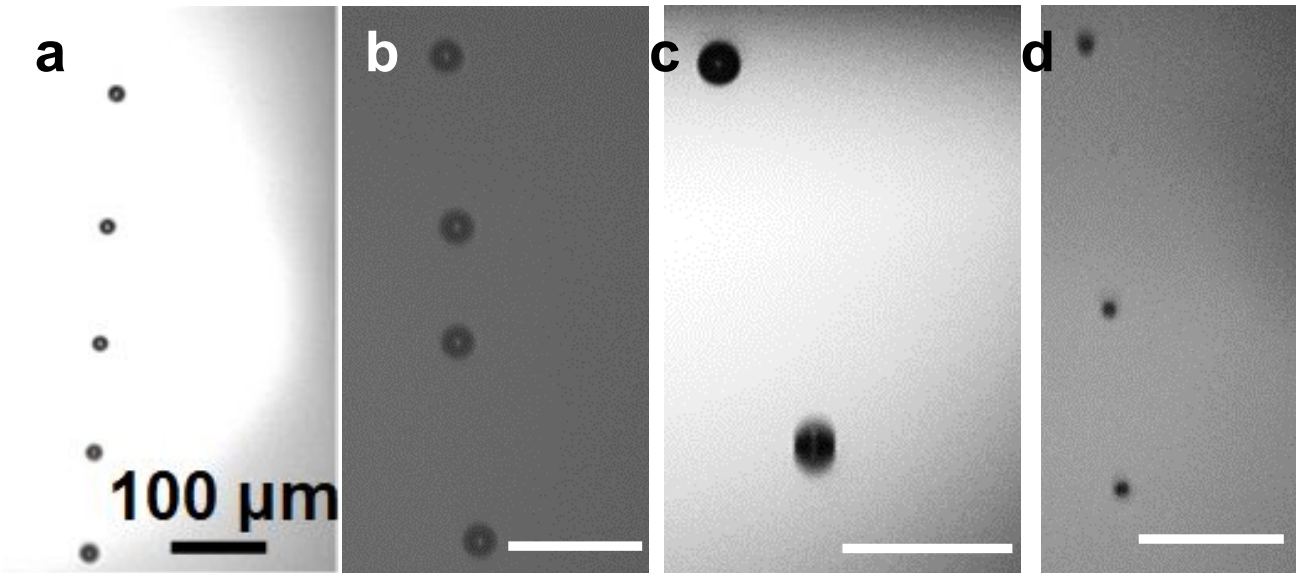

Figure S1. Strobe images for monodisperse droplets for (a) water, (b) ethanol, (c) hexane, and (d) dodecane.

S.3. Calculation of Interfacial Temperatures

The interfacial temperatures were calculated using Eq. (S1)[2]:

$$T_{\text{int}} = T_{\infty} - \frac{h_{\text{fg}} D_{\text{va}} M P_{\text{v,int}}}{k_{\text{f}} R T_{\infty}}, \tag{S1}$$

where h_{fg} is the latent heat of evaporation of the evaporating fluid, D_{va} is the diffusion coefficient of the vapor of the evaporating fluid (subscript v) in air (subscript a), M is the molecular mass of the evaporating fluid, $P_{\text{v,int}}$ is the vapor pressure at the interface, k_{f} is the thermal conductivity of the evaporating fluid, R is the universal gas constant and and T_{∞} is the room temperature. This section describes how the temperature dependent properties were obtained in order to carry out the iterations.

S.3.1. Calculation of Vapor Pressure. Vapor pressure values were calculated using Antoine's equation (Eq. (S2)) using the respective coefficients for each working fluid[3]. These coefficients are given in Table S1[4]. Here, the obtained vapor pressure values are in mmHg, and the input temperatures are in ℃.

$$P_{\text{v}} = 10^{A - \frac{B}{T + C}}, \tag{S2}$$

Table S1. Coefficients for Antoine's equation for different working fluids.

	Water	**Ethanol**	**Hexane**	**Dodecane**
A	8.07131	8.20417	7.01051	6.98
B	1730.63	1642.89	1246.33	1626
C	233.426	230.3	232.988	180.311

S.3.2. Calculation of Latent Heat of Vaporization. Enthalpy of vaporization was calculated differently for each working fluid. For water, the slope of the Clasius - Clapeyron relation (Equation 9 of the main text) and Equation S2 were utilized. For the low surface tension fluids, latent heat of vaporization was calculated using Eq. (S4)[5]:

$$h_{\mathrm{fg}} = A * \exp\left(-\alpha \frac{T}{T_{\mathrm{c}}}\right)\left(1 - \frac{T}{T_{\mathrm{c}}}\right)^{\beta}, \tag{S3}$$

where h_{fg} is given in kJ/mol T is given in K. the coefficients A, α, T_{c} and β are given in Table S2. For dodecane, tables were used.

Table S2. Coefficients to calculate the latent heat of vaporization for low surface tension fluids.

	Ethanol	**Hexane**
A (kJ/mol)	50.43	43.85
$\boldsymbol{\alpha}$	-0.4475	-0.039
$\boldsymbol{T_{\mathrm{c}}}$ **(K)**	513.9	507.4
$\boldsymbol{\beta}$	0.4989	0.397

S.3.3. Calculation of Mass Diffusivity in Air. The diffusion coefficients were calculated differently for each working fluid at the film temperatures ($(T_{\mathrm{int}} + T_{\infty})/2$). For water, Eq. (S5) was employed[6]:

$$D_{va} = D_{\mathrm{ref}}\left(\frac{T}{T_{\mathrm{ref}}}\right)^{m}\left(\frac{P}{P_{\mathrm{ref}}}\right), \tag{S5}$$

where D_{ref} = 19.7 mm^2/s, T_{ref} = 256 K and P_{ref} = 101 kPa. For the low surface tension fluids, tables were used to calculate the mass diffusivity values.

S.3.4. Calculation of the Temperature of the Interface. The thermal conductivity values of the fluids were calculated using the tables. Then, Eqs. (S2-S5) were combined with the table values and used in Eq. (1) in an iterative procedure to solve for T_{int}. For T_{∞} = 297 K, ϕ = 0.5 where ϕ is the relative humidity (only important for water) and P = 1 atm; we obtain T_{int} = 22.8 ℃ for water, T_{int} = 17.5 ℃ for ethanol, T_{int} = 14 ℃ for hexane, and T_{int} = 23.8 ℃ for dodecane.

Considering the volatility of these fluids, the results make sense as the most volatile one suffers the most from self-cooling effects while the non-volatile ones show negligible cooling.

S.4. Thermal Resistance Analysis

Four different heat transfer mechanisms play an important role in droplet evaporation in the absence of Marangoni and convection effects; namely, 1) Heat transfer from the base substrate to the droplet, 2) Conduction of heat within the droplet, 3) Conduction of heat with the surroundings at the liquid-vapor interface, 4) Diffusion of water vapor molecules once they evaporated in the vicinity of the interface.

The resistance to heat transfer from the base substrate to the droplet depends on the coatings, uniformness of temperature, contact area and the epitaxiality of the contact. We have showed in the manuscript that the presence of the droplet does not induce any temperature gradients on the surface of the base substrate. Furthermore, we will assume epitaxial contact, i.e. no contact resistance between the droplet and the substrate. With these assumptions, we can easily calculate the thermal resistance of the droplet base for a 1D slab ($R_{\text{th,base}} = {}^{L}/_{k A_{\text{b}}}$, where L is the thickness of the coating, k is the thermal conductivity of the coating and A is the contact area)[7]. Further assuming a spherical block, we obtain $R_{\text{th,base}} \approx {}^{L}/_{k\pi {R_{\text{b}}}^2}$. This result is valid for the hydrophilic sample (Si-Au, where there is a 10 nm thick gold coating with $k =$ 310 W/mK) and the coated unstructured hydrophobic sample (Si-TFTS, where there is a 1 nm thick TFTS coating with $k =$ 0.15 W/mK). However, the presence of nanostructures makes the analysis more complicated. For nanostructured surfaces, the pillars become important as the air pockets and/or fluid filling between the pillars alter the heat transfer characteristics (Figure S2). Miljkovic et al. showed that for a droplet on a nanostructured surface, the resistance to heat transfer with the base substrate is given by[8]:

$$R_{\text{th,base}} = \frac{1}{\pi R^2 \sin^2\theta k_{\text{HC}}}\left(\frac{k_{\text{P}}\varphi}{\delta_{\text{HC}}k_{\text{P}} + h_{\text{P}}k_{\text{HC}}} + \frac{k_{\text{f}}(1-\varphi)}{\delta_{\text{HC}}k_{\text{f}} + h_{\text{P}}k_{\text{HC}}}\right)^{-1} \tag{S4}$$

where the subscripts HC, P and w denote hydrophobic coating, pillar and water, respectively, and φ is the solid fraction, h is the height and δ is the thickness. For our superhydrophobic sample (Cu-HTMS), the hydrophobic coating is HTMS ($\delta_{\text{HC}}\sim$ 1 nm, $k_{\text{HC}} \approx$ 0.15 W/mK), the pillar is

the oxidation layer of copper oxide ($h_P \approx 1$ μm, $k_P \approx$ 33 W/mK) and $\varphi = \pi d^2/4l^2 \approx 0.05$ with the pillar diameter $d \approx$ 100 nm and center-to-center pillar spacing $l \approx$ 1 μm.

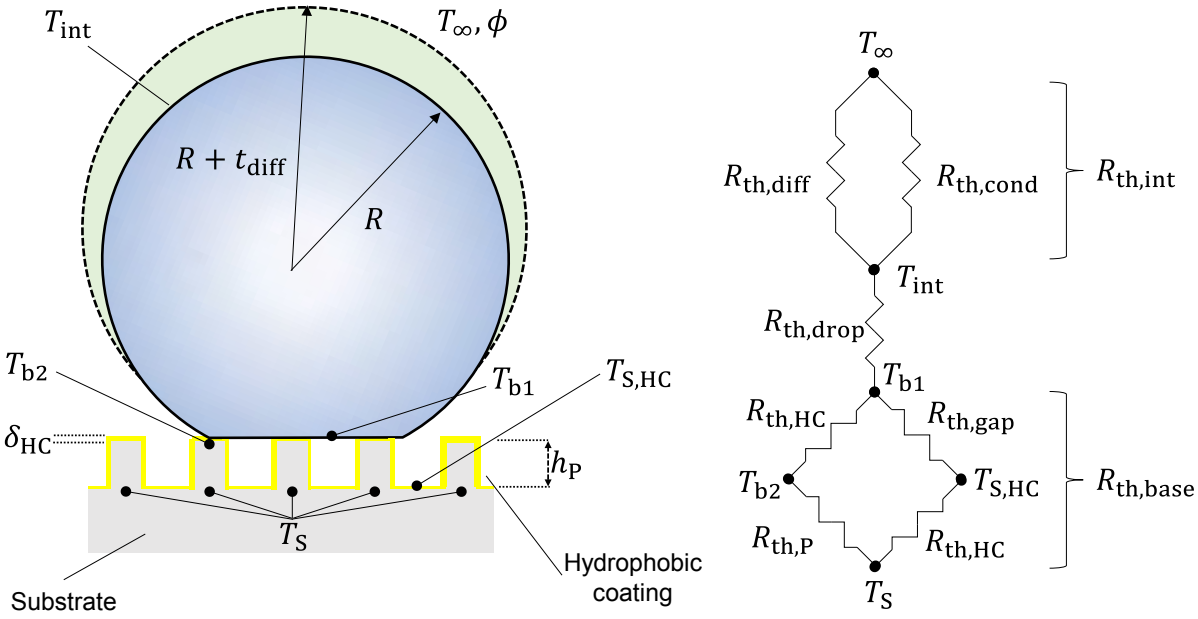

Figure S2. Schematic of an evaporating droplet on a superhydrophobic structured surface and the resistance analogy.

The transferred heat from the base will be transported via conduction within the droplet, which was calculated by Miljkovic et al. as $R_{th,drop} \approx \theta/4\pi R k_f sin\theta$, where θ is the contact angle of the droplet, R is the droplet radius of curvature and k_f is the thermal conductivity of the working fluid (Wenzel state) or air (Cassie-Baxter state)[8].

Heat to evaporate the droplet can also be supplied from the surroundings at the liquid-vapor interface via conduction. The resistance at the liquid-vapor interface to conduction can be calculated as $R_{th,cond} = 1/(4\pi k_{air} R)$ where k_{air} is the thermal conductivity of air.

Another mechanism governing evaporation is vapor diffusion. The resistance of vapor molecules in air to diffusion is given as $R_{diff} = 1/4\pi D_{va}(1/R - 1/R + t_{diff})$ where D_{va} is the diffusion coefficient of vapor in air and t_{diff} is the diffusion length for a stationary medium assumption[7]. We can estimate t_{diff} from Fick's Law of Diffusion. Using Eq. (7) of the main text and experimentally measured evaporation rates, $t_{diff} \approx D_{va}(\rho_{int} - \rho_\infty)/\dot{m}''$, where $\dot{m}''$ is the evaporative flux obtained by normalizing the rate of evaporation with the interfacial area, and int

and ∞ represent the interface and the surroundings, respectively. We now define density in terms of known parameters $\rho = {M_{\mathrm{w}}\phi P_{\mathrm{v}}}/{R_{\mathrm{g}}T}$, where M_{w} is the molecular mass of the working fluid, ϕ is the relative humidity (assumed equal to 1 at the interface, 0.5 in the surroundings due to experimental conditions for water and 0 for other working fluids since they do not have concentrations in ambient air), P_{v} is the vapor pressure of the working fluid, and R_{g} is the universal gas constant. Solving these parameters yields the resistance of vapor molecules to diffusion. Note that this is not a thermal resistance and needs to be converted. Defining an effective diffusive thermal conductivity value ($k_{\mathrm{diff}} = \rho_{\mathrm{v}} C_{\mathrm{p},v} D_{\mathrm{va}}\mathrm{Le}$, where v denotes vapor properties and Le is the Lewis number) and replacing with the diffusion coefficient D_{va}, we obtain the thermal resistance due to vapor diffusion near the liquid-vapor interface ($R_{\mathrm{th,diff}} = {1}/{4\pi k_{\mathrm{diff}}}({1}/{R} - {1}/{R + t_{\mathrm{diff}}})$. Note that this resistance is temperature dependent. The interfacial temperatures are known to be morphology dependent. For a superhydrophobic droplet, most of the interface will be at a self-cooled value, while for a hydrophilic droplet it will be warmer. Therefore, in order to carry out the numerical analysis, we will assume $T_{\mathrm{int}} = T_{\mathrm{wb}}, \theta > 90°$ and $T_{\mathrm{int}} = 0.5(T_{\mathrm{wb}} + T_{\mathrm{s}}), \theta < 90°$ where T_{wb} is the wet bulb temperature at the given atmospheric conditions and T_{s} is the temperature of the heated substrate. After calculating $R_{\mathrm{th,diff}}$, $R_{\mathrm{th,int}} = ({1}/{R_{\mathrm{th,diff}}} + {1}/{R_{\mathrm{th,cond}}})$.

S.5. Contact Angle Variations of Surfaces with Increasing Temperature

The variations in the contact angles for the used surfaces are given in Figure S3. It is seen that variations are negligible (< 10%) for each tested surface and working fluid.

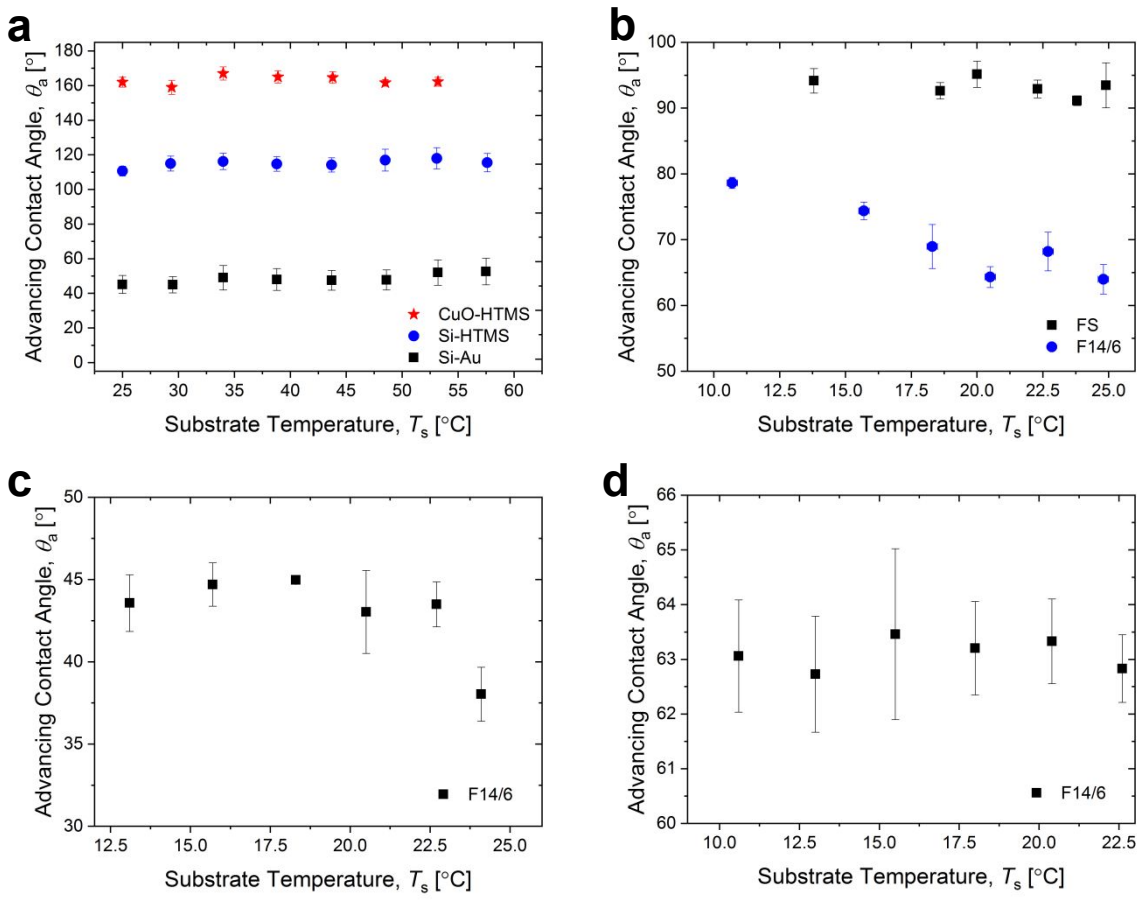

Figure S3. Variations in the contact angle with changing sample temperatures for (a) water, (b) ethanol, (c) hexane, and (d) dodecane for every tested sample.

S.6. Effect of Relative Humidity on Rate of Evaporation

Following the logic given in the main manuscript (Section 3.5), experiments were performed on water which is naturally present in ambient air. The results are given in Figure S4. The predicted linearly decreasing behavior is observed due to the lower concentration gradients with increasing relative humidity. Additional experiments for ethanol and dodecane were also performed and it is seen that relative humidity has negligible effect on evaporation dynamics, since vapors of ethanol and dodecane do not naturally have any concentrations in ambient air (Figure S5).

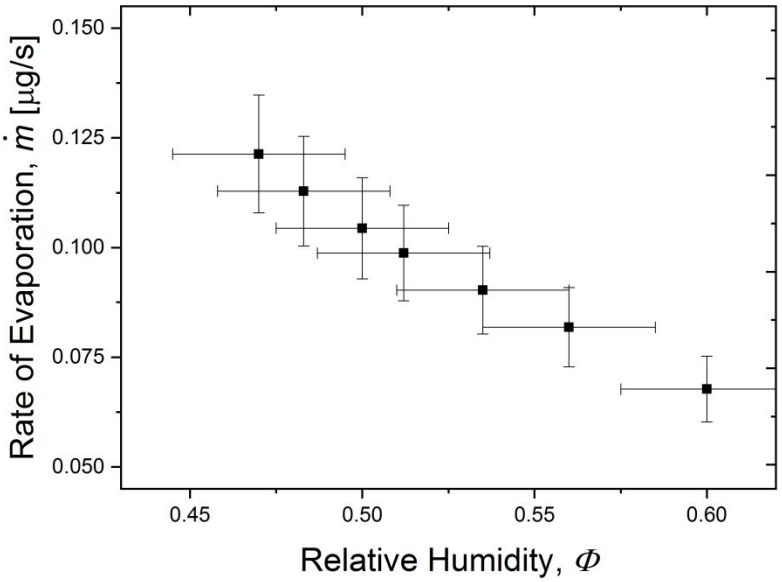

Figure S4. Rate of evaporation as a function of relative humidity. Rate of evaporation decreases linearly for increasing relative humidity due to decreasing concentration gradients of water vapor molecules.

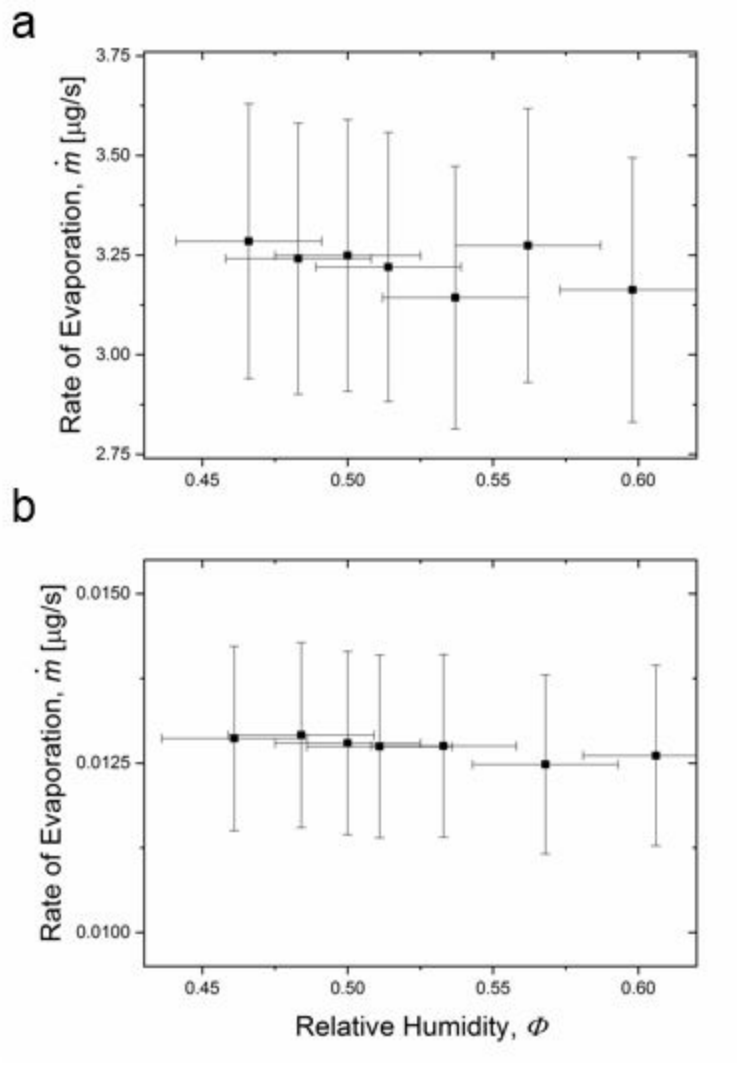

Figure S5. Rate of evaporation as a function of relative humidity for (a) ethanol and (b) dodecane. Rate of evaporation is insensitive to the changes in relative humidity for both working fluids (STD $\approx$ 1.7% for Ethanol and $\approx$ 1.2% for dodecane where STD refers to standard deviation from the mean value).

S.7. Interfacial Area

The normalized liquid-vapor interfacial surface area (normalized by the total surface area of a sphere, $4\pi R^2$) is plotted in Figure S6 as a function of droplet contact angle for a constant droplet radius of curvature. It is seen that the interfacial surface area increases as the contact angle increases, affecting the evaporation dynamics.

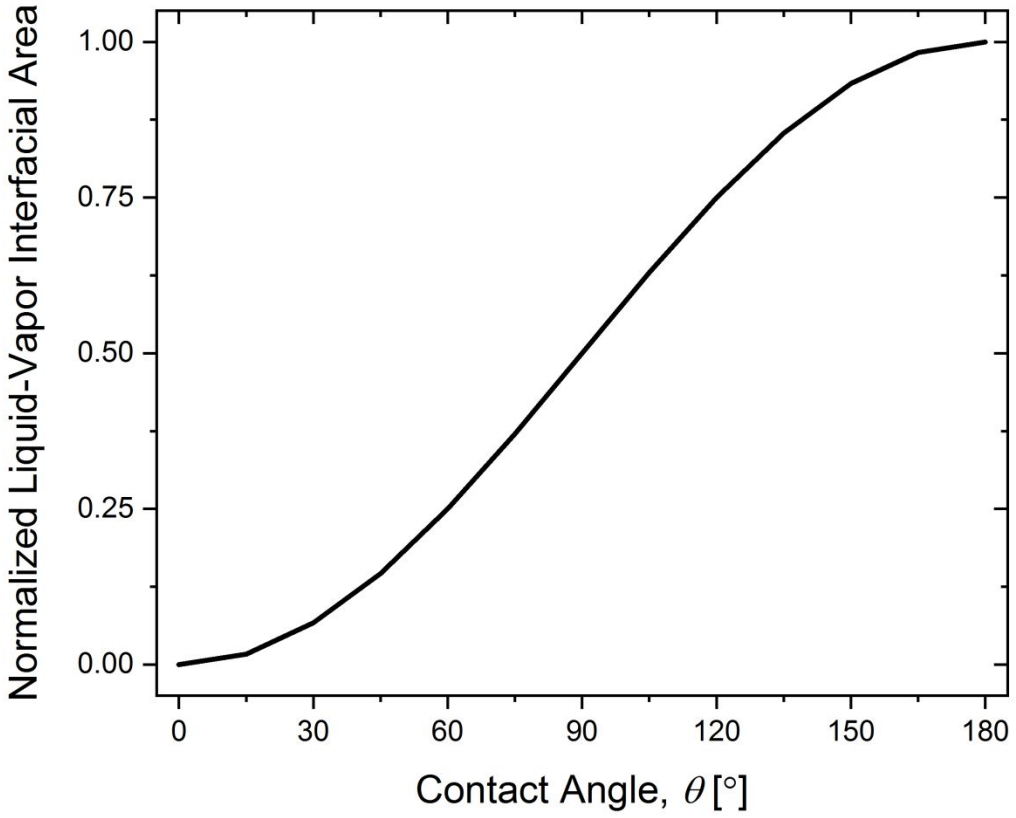

Figure S6. Normalized liquid-vapor interfacial surface area as a function of droplet contact angle for a constant droplet radius of curvature. The interfacial area is normalized by the total surface area of a sphere ($4\pi R^2$). It is seen that as the droplets become non-wetting (higher contact angle), the interfacial area increases.

S.8. Uncertainty Associated with the Experiments

The experimental uncertainties associated with the experimental apparatus and the procedures are given in Table S3.

Table S3. Uncertainties associated with experimental measurements.

Measurement	Symbol	Instrument	Span	Uncertainty
Apparent Contact Angle	θ	Microgoniometer	0 - 180°	$\pm$ 1° (minimum)
Dispensing Droplet Size	V_{d}	Microgoniometer	3 pL	$\pm$ 0.3 pL
Measured Rate of Evaporation	$\dot{m}$	Microgoniometer	0 – 15 µg/s	$\pm$ 11%
Ambient Temperature	T_{∞}	Hygrometer	-30 to 75℃	$\pm$ 0.6℃
Relative Humidity	ϕ	Hygrometer	0 – 100%	$\pm$ 2.5%
Chiller Temperature	T_{c}	Circulator	-30 to 200℃	$\pm$ 1℃
Surface Temperature	T_{s}	K-Type Thermocouple	0 - 100℃	$\pm$ 1.5℃

References

1. Enright, R.; Miljkovic, N.; Sprittles, J.; Nolan, K.; Mitchell, R.; Wang, E. N., How Coalescing Droplets Jump. *ACS Nano* **2014,** *8* (10), 10352-10362.
2. Erbil, H. Y.; Dogan, M., Determination of Diffusion Coefficient−Vapor Pressure Product of Some Liquids from Hanging Drop Evaporation. *Langmuir* **2000,** *16* (24), 9267-9273.
3. Antoine, M. C., Nouvelle Relation Entre les Tensions et les Temperatures. *C. r. held Seanc. Acad. Sci. Paris* **1888,** *107*, 681-684.
4. *NIST Chemistry WebBook, NIST Standard Reference Database Number 69*. National Institute of Standards and Technology: 2005.
5. Majer, V., Enthalpies of vaporization of organic compounds : a critical review and data compilation. Svoboda, V.; Kehiaian, H. V., Eds. Blackwell Scientific Publications: Oxford [Oxfordshire] ;, 1985.
6. Park, T.; Rettich, T. R.; Battino, R.; Wilhelm, E., Binary gaseous diffusion coefficients VI. Chlorobenzene. 1,2-dichlorobenzene. 1,3-dichlorobenzene, 1,1,1-trichloroethane, tetrachloroethene, 1,4-dioxane and octamethylcyclotetrasiloxane with air at 1 atm and 283 k to 343 k. *Materials Chemistry and Physics* **1987,** *16* (5), 397-410.
7. Incropera, F.; DeWitt, D., Introduction to heat transfer. **1985**.
8. Miljkovic, N.; Enright, R.; Wang, E. N., Effect of droplet morphology on growth dynamics and heat transfer during condensation on superhydrophobic nanostructured surfaces. *ACS nano* **2012,** *6* (2), 1776-1785.